



Assessing the impacts of land-use/land-cover change on the development of urban heat island effects

Murat Atasoy¹

Received: 20 May 2019 / Accepted: 23 November 2019 / Published online: 29 November 2019
© Springer Nature B.V. 2019

Abstract

Urban heat island (UHI) has been a detrimental problem over the last decades. Also, climate change has obtained more attention due to increased urbanization. Turkey is one of the countries experiencing a rapid urbanization which has resulted in significant UHI impacts on the regional climate and environment. This study was conducted in Osmaniye city, Turkey, where there is a need to determine the effects of land-use/land-cover changes (LUCC) on the UHI using Landsat images. The geospatial analyses were undertaken using USGS/NASA Enhanced Thematic Mapper Plus geospatial data from 2000 to 2018. The results showed that percent cover of urban areas significantly increased from 6.13 to 17.76%, broad-leaved forest cover decreased from 14.2 to 11.6%, road and rail network cover increased from 5.23 to 10.85%, and coniferous forest cover decreased from 15.85 to 9.02% between 2000 and 2018. During the process of urbanization from 2000 to 2018, most of the bare land cover was converted to agricultural lands and urbanized areas due to vegetative degradation, and industrial units cover increased from 7.76 to 9.53%. The land surface temperature was 35.57 °C for approximately 25% of the study area in 2000, while the same temperature was calculated for 76% of the study area in 2018. The results suggest that LUCC from vegetation to urbanized areas has significantly increased the land surface temperature. This implies that the application of remote sensing technique could help to design methods to mitigate UHI effects by estimating future land-use/land-cover change in urban areas.

Keywords Land surface temperature · Land-use/land-cover change · Remote sensing · Urban heat island · Urbanization in Turkey

1 Introduction

The estimates by the United Nations show that 60% of the world will be affected by urbanization by 2030 (Chun and Guldmann 2014). In recent years, one of the fundamental reasons of the climate change is the decrease in natural cover and substantial growth

✉ Murat Atasoy
muratatasoy@osmaniye.edu.tr

¹ Faculty of Architecture, Design, and Fine Arts, Osmaniye Korkut Ata University, 80000 Osmaniye, Turkey

of urbanization (Hosseini et al. 2015). Urban Heat Island (UHI) phenomenon is one of the most significant factors associated with this rapid urban growth around cities (Mirzaei 2015; Bokaie et al. 2016). The UHI was first appraised by Howard (1833), and the subject has gained momentum in the following years (Laosuwan and Sangpradit 2012). An UHI is a landscape that has specific warmth of the surface in comparison with its surroundings (Agbor and Makinde 2018). The fundamental driving factors of UHIs are alterations in land surface structure, energy utilization, and increase in impervious surfaces such as constructions, buildings, and concrete pavements leading to heat accumulation (Bilgili et al. 2013; Güngör and Polat 2017; Büyükebeşe and Aslan 2019).

The features of UHI have been comprehensively examined by scientists. For instance, Deosthali (2000) reported that urban city centers show the characteristics of heat and moisture landscapes at night, and heat and dry landscapes during the early hours of the day. For more local studies, Chen et al. (2002) introduced a satellite perspective to assess the UHI and Land Surface Temperature (LST) using Landsat Thematic Mapper (TM) at 120 m resolution, and Enhanced Thematic Mapper Plus (ETM+) geospatial data at 60 m resolution (Chen et al. 2006).

Furthermore, the total built-up area and the increase in impervious surface cause an adverse impact on UHI intensity and high thermal capacity (Dwivedi and Mohan 2018). UHI intensity is also significantly influenced by land-use/land-cover changes (LUCC) such as vegetation distribution, urban–suburban transitions, and urban–wild land interface (Bokaie et al. 2016). In order to establish a relationship between LUCC and UHI intensity, digitizing large spectral range satellite imagery and developing thermal UHI maps help providing the required data for the studies (Feizizadeh et al. 2013).

This study aimed at assessing the LUCC associated with the UHI impact since 2000 in Osmaniye city, Turkey, where there is need to determine influences of LUCC on the UHI using Landsat satellite images. The main objectives of this study are: (1) to derive a LST map using ETM+ thermal bands for the years of 2000 and 2018, (2) to investigate the LUCC during the aforementioned period, and (3) to evaluate the relationship between UHI intensity and LUCC in the study area over time.

2 Materials and methods

2.1 Study area

The current study was conducted in the city of Osmaniye, Turkey (Fig. 1). Osmaniye is located between 37.0746° N and 36.2464° E. The city is lowland and flat with a hilly surrounding border. The altitude of Osmaniye is approximately 121 m above sea level, and the weather conditions vary considering the topography. The climate of the study area is warm and temperate. Osmaniye has an annual average temperature at 18.2 °C, and the highest annual temperature is 42.8 °C (Atasoy 2018; Osmaniye Municipality 2018). The area of Osmaniye is 3222 km², and the population density is 527,724 with 164 people per km² (Soysal et al. 2010; TUIK 2018).

2.2 Land Surface Temperature (LST) Analysis

For the present study, USGS/NASA Enhanced Thematic Mapper Plus (ETM+) geospatial data obtained on January 11, 2018, were used. The data were obtained for the years

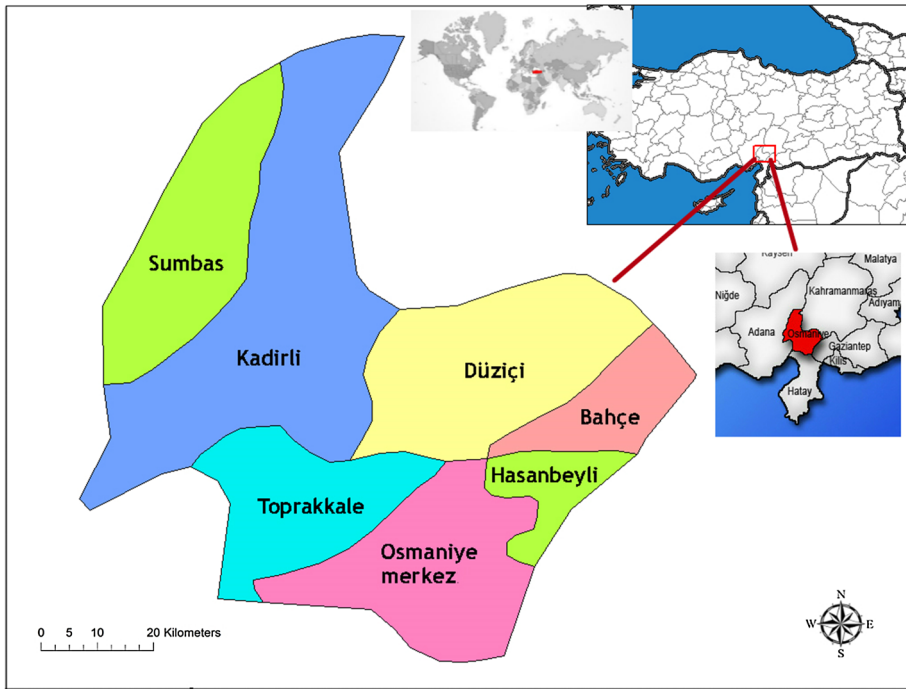


Fig. 1 Location of the Osmaniye city and its towns

2000 and 2018 which include the most accurate information for the study area. The satellite images were chosen within cloud coverage less than 10% to increase the geospatial analysis robustness. The weather conditions such as air temperature, humidity, and wind at time of sensor condition were uniform for the study period of 2000 and 2018 which were selected to retrieve proper data and images. Also, ENVI software was used to reduce the influences of atmospheric conditions on the satellite images and to correct errors. Then, Dark Object Subtraction (DOS) method was applied which analyzes the darkest pixel value, and values greater than zero are considered as atmospheric scattering (Bokaie et al. 2016). The satellite images were re-projected to WGS84/UTM coordinate system. To perform radiometric modifications and convert the Digital Numbers (DN) of image pixels, ETM+ band 10 and band 11 were used to apply the following equation (Chander et al. 2009; Sun et al. 2010):

$$L(\lambda) = \left(\frac{L_{\text{Max}} - L_{\text{Min}}}{255} \right) \times \text{DN} + L_{\text{Min}} \quad (1)$$

where $L(\lambda)$ is the radiance in ($\text{W}/\text{m}^2/\text{sr}/\text{mm}$), L_{Max} is the maximum value of spectral radiance, L_{Min} is the minimum value of spectral radiance in ($\text{W}/\text{m}^2/\text{sr}/\text{mm}$), and 255 is the maximum calibrated digital number value in image, and DN is the calibrated pixel digital number.

Then, the brightness temperature was calculated using the following equation (Dwivedi and Mohan 2018):

$$T = \frac{K_2}{\ln\left(\frac{K_1}{L_\lambda} + 1\right)} - 273.15 \quad (2)$$

where T is the radiance temperature in degrees Celsius, K_1 and K_2 are thermal calibration constant values, and L_λ is the top of atmosphere radiance of the sensor in ($\text{W}/\text{m}^2/\text{sr}/\text{mm}$).

In order to estimate LST, land surface emissivity which is an important factor predicting the emitted radiance was calculated (Agbor and Makinde 2018). The equation used for the emissivity calculation is as follows (Agbor and Makinde 2018):

$$\varepsilon = \varepsilon_s \lambda + (\varepsilon_v \lambda - \varepsilon_s \lambda) P_v \quad (3)$$

where ε is the calculated emissivity, ε_v and ε_s represent soil and vegetation emissivity, respectively, and ε_v is the fraction of vegetative cover.

P_v value is derived from the Normalized Difference Vegetation Index (NDVI) calculation which indicates a Simple Ratio (SR) formulated as follows (Fung and Siu 2000):

$$\text{NDVI} = \frac{\text{NIR} - R}{\text{NIR} + R} \quad (4)$$

$$P_v = \left(\frac{\text{NDVI} - \text{NDVI}_{\min}}{\text{NDVI}_{\max} - \text{NDVI}_{\min}} \right)^2 \quad (5)$$

where NIR is the near-infrared reflectance and R indicates the visible red reflectance. As a numerical indicator, the NDVI is used as a proxy measure for pixel vegetation cover for emissivity calculation in a large body of LST studies (Fung and Siu 2000).

After calculation of the land surface emissivity, the following equation was applied to estimate the LST (Weng and Lu 2008):

$$\text{LST} = (T / (1 + (0.00115 * T / 1.4388) * \ln(\varepsilon))) \quad (6)$$

where LST is the Land Surface Temperature, T is the brightness temperature in degrees Celsius, and ε is the calculated band emissivity.

2.3 Land-use/land-cover Change (LUCC) Classification and Accuracy

Satellite images are commonly used to create the LUCC maps in geospatial data relevant studies. The LUCC maps often include images which have values of various pixels to classify Landsat data (Lobo et al. 2004). For the present study, USGS/NASA ETM+ geospatial data from 2000 and 2018 were used to evaluate the correlation between LST and LUCC with the most available satellite images.

For this purpose, the LUCC maps were classified into nine different land-use classes: (1) urban areas, (2) road and rail networks, (3) industrial units, (4) pasture lands, (5) agricultural lands, (6) broad-leaved forest, (7) coniferous forest, (8) watercourses, and (9) bare land using supervised classification method (Bokaie et al. 2016). Land-use/land-cover classes were defined from satellite images obtained in 2018 by visual interpretation through ArcGIS 10.3. Visual interpretation can provide more accurate results in contrast to computer-based estimation of remote sensing images (Yang et al. 2017; Atasoy et al. 2018). For the present study, land-use/land-cover classes of each patch were determined considering the size, shape, color, and neighborhood relationship of the patch. Patches

which could not be identified were combined with aerial photographs and other data features such as soil type, vegetative composition of each patch, digital elevation model, and climate data to classify the land use. As applied in both Yang et al. (2017) and Bokaie et al. (2016)'s studies, ten classes of LUCC were defined for the study area in a combination of both geospatial analysis and field visits.

Due to the low resolution of images, classification requires the validation of data accuracy. Therefore, the Kappa coefficient was used to calculate the accuracy of data applied in the classification of pixels in comparison with ground-truth with the following equation (Congalton 1991):

$$K = \frac{N \sum_{i=1}^r x_{ii} - \sum_{i=1}^r (x_{i+} * x_{+i})}{N^2 - \sum_{i=1}^r (x_{i+} * x_{+i})} \quad (7)$$

where K and r represent the Kappa coefficient and the number of rows in the error matrix, respectively, x_{ii} is the observation numbers in row i and column i , x_{+i} is the total number of observations in the i th column, and N represents the total number of observations.

To implicate the Kappa coefficient, a total of 1063 sample points were randomly selected across the study area, and they were relatively and uniformly distributed among the LUCC classes. The LUCC was compared using post-classification map comparison method.

3 Results

The results of the analyses showed that the calculated classification accuracy was 93.24%, and Kappa statistics was 0.91. The supervised classification error matrix results are shown in Table 1. Also, the spatial pattern of the UHIs has shifted from a scattered pattern (agricultural land, bare land, pasture land, and urban areas had higher temperatures than other area types) in 2000 to adjacent pattern of UHIs in 2018 and land conversion to urbanized areas (Fig. 2a, b). The centers of UHIs were associated with urban areas and deforested

Table 1 Accuracy evaluation of classification in LUCC maps

Class name	Reference total	Classified total	Number correct	Producers accuracy	Users accuracy
Urban areas	125	123	121	96.8	98.4
Road and rail networks	115	112	110	95.6	97.3
Industrial units	85	84	82	96.4	98.8
Pasture lands	134	132	130	97	98.5
Agricultural lands	128	125	124	96.8	97.6
Broad-leaved forest	66	64	61	92.4	96.9
Coniferous forest	89	88	87	97.7	98.8
Mixed forest	117	116	114	97.4	99.1
Water courses	62	59	58	93.5	95.1
Bare land	142	140	139	95.2	98.5

Calculated classification accuracy is 93.24%, and Kappa statistics is 0.91

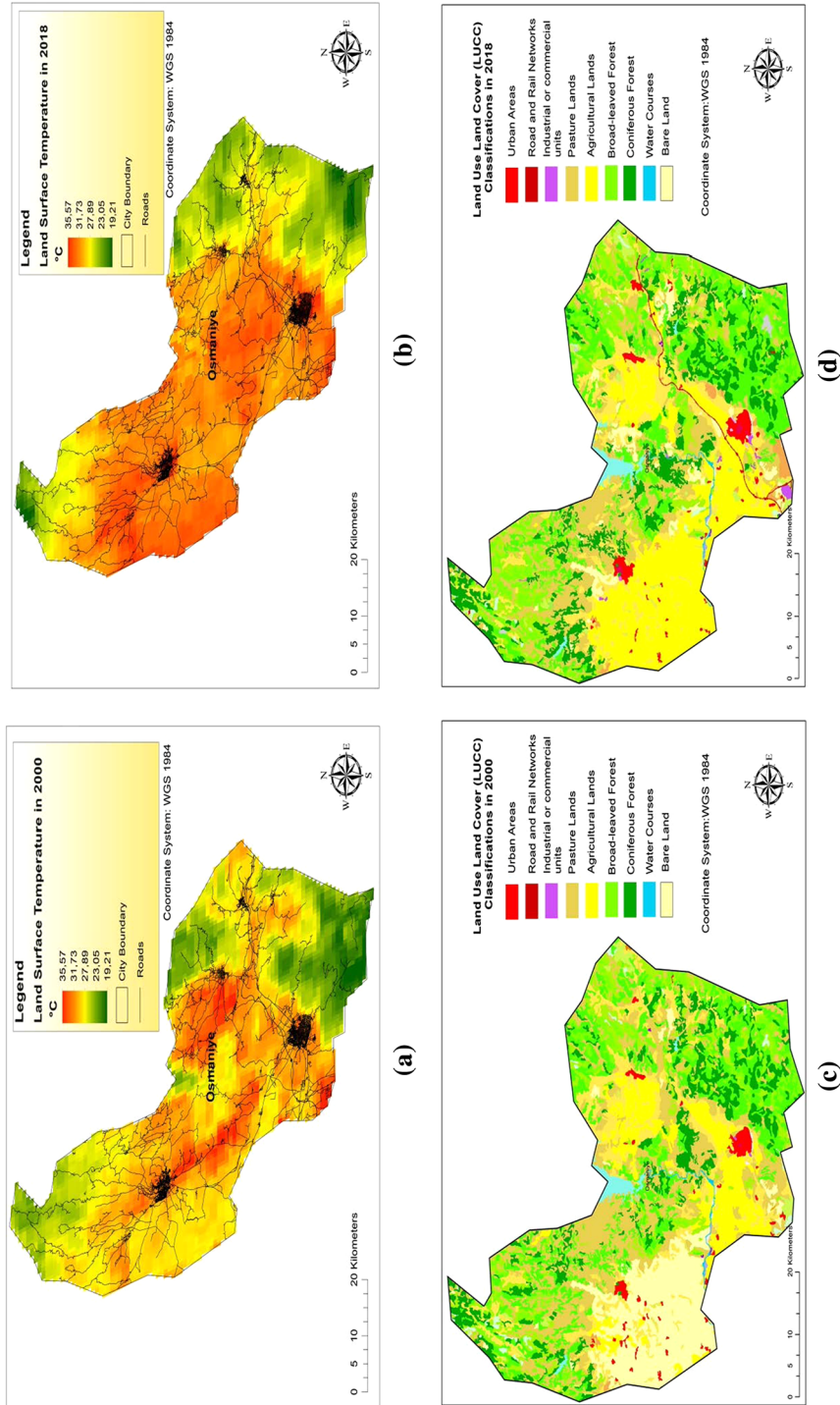


Fig. 2 LUCC pattern and land surface temperature distribution in Osmaniye city for 2000 and 2018: **a** land surface temperature in 2000, **b** land surface temperature in 2018, **c** LUCC pattern in 2000, and **d** LUCC pattern in 2018

lands which can be derived by comparing LUCC maps with land surface temperature maps (Fig. 2a vs. c, and Fig. 2b vs. d).

According to the geospatial analysis results of (ETM+) images, distribution of urban areas has changed from a scattered pattern in 2000 in comparison with a mass pattern in 2018 with an increase in urban infrastructure system in the city of Osmaniye. Also, the comparison of land-use/land-cover classes obtained from images of 2000 and 2018 has revealed that bare lands shifted to agriculture lands and urbanized areas (Fig. 2c, d).

A more serious concern was the degradation of coniferous and deciduous forest between 2000 and 2018 in the central section of the study area. This shift in forest conditions over such a short period was also associated with the increase in land surface temperature between 2000 and 2018. Also, in the dotted urban area shown in Fig. 2c a significant proportion is bare soil, which was converted to agriculture (Fig. 2d).

The analysis of LUCC showed a significant percentage-wise change between images of LUCC in 2000 and 2018. The percent cover of urban area increased from 6.13% in 2000 to 17.76% in 2018, while broad-leaved forest cover decreased from 14.2% in 2000 to 11.6% in 2018. Road and rail network cover increased from 5.23% in 2000 to 10.85% in 2018, whereas coniferous forest cover significantly decreased from 15.85% in 2000 to 9.02% in 2018. During the process of urbanization from 2000 to 2018, most of the bare land cover has been converted to agricultural lands and urbanized areas, and also industrial units cover increased from 7.76 to 9.53% due to vegetative degradation (Table 2).

Overall, the results of geospatial analysis revealed that land-use change from broad-leaved and coniferous forest cover to urbanized areas significantly increased the temperature between 2000 and 2018 in the study area. Based on the percentage estimate, the highest calculated LST temperature was 35.57 °C for approximately 25% of the study area in 2000, while the same temperature value was calculated for 76% of the study area in 2018 (Fig. 2a, b).

4 Discussion

Considering the variability in forms of urban landscapes, different urban planning can result in varieties in forms of heat islands and their interrelations. Although there have been some other researches addressing the negative impacts of urbanization in city of Osmaniye (Kilinc and Gulersoy 2011; Yalcin 2014), this study is the primary research which evaluated the correlation between UHI and LUCC pattern for the said city. While densely populated areas are commonly warmer than the surrounding areas, land-use change patterns can negatively influence the temperature fluctuations (Fu and Weng 2017; Li et al. 2018). In this study, based on the geospatial analysis, it was found that UHI intensity was influenced by land-use changes from agricultural lands to urbanized areas (Fig. 2a–d). This high degree of the land conversion process in the study area such as agricultural development during the study period was supported by the Ministry of Agriculture and Forestry of Turkey (Osmaniye Municipality 2018). The results of UHI analysis also showed that multi-core population centers can exhibit multi-core UHI, and these results were consistent with Bokaie et al. (2016) and Yuan and Bauer (2007) findings.

The results of this study were consistent with several researches reporting that a strong relationship can occur between UHI and LUCC in urban areas. For instance, Estoque et al. (2017) examined the relationship between UHI and spatial distribution of urban green spaces in Southeast Asia and found that increase in impervious surface could result in

Table 2 LUCC (%) in study area from 2000 to 2018

Land-use/land-cover classes	Urban areas	Road and rail network	Industrial units	Pasture lands	Agricultural lands	Broad-leaved forest	Coniferous forest	Water courses	Bare land
2000 (%)	6.13	5.23	7.76	10.03	6.23	14.2	15.85	12.45	22.12
2018 (%)	17.76	10.85	9.53	3.89	16.24	11.6	9.02	11.81	9.30
Changes (%)	11.63	5.62	1.77	6.14	10.01	2.6	6.83	0.64	12.82

LUCC percent data were calculated by dividing the total study area cover percent into the pixel area cover of a given land-use/land-cover type

urban green space degradation, thus elevating surface temperature in Jakarta and Manila. Furthermore, Li et al. (2011) and Nastran et al. (2018) assessed the correlation among the planning of urban landscape structure, urban green land use, and UHI pattern. The studies concluded that landscapes with higher proportion and edge density of urban green spaces have lower land surface temperature and UHI influence than urban vegetation with lower proportion and edge density in urban–rural gradients.

Increase in green space surrounding urban city centers can reduce the UHI impact which is fundamentally driven by air pollution, heat release from air conditioners, vehicles, and lots of other artificial heat resources in suburban areas (El-Hattab et al. 2017). Considering the temperature changes between years 2000 and 2018, broad-leaved and coniferous forest cover around Osmaniye city center and suburban areas have been degraded by increase in the total built-up area; thus, this alteration can be the most significant driving force of temperature accumulation around multi-core UHI areas in Osmaniye (Table 2, Fig. 2). Even though the bare land cover also changed with agricultural and pasture lands, the extent and increase in built-up lands may pioneer the UHI effect during the 2000–2018 period in the study area.

During the accuracy assessment of satellite images, the panchromatic bands of various satellite sensors such as Landsat-7 ETM+ and Landsat-8 OLI can be used as a reliable reference. Also, the panchromatic bands are commonly used in LUCC studies due to consistency with TIR bands (Estoque and Murayama 2015). This paper argued that although bare lands in 2000 have changed with agricultural and pasture lands in 2018, UHI effect significantly increased due to the increase in urbanized areas and reduction in forest cover of the study area. Therefore, as the results demonstrate, the proposed relationship between land surface temperature increase and LUCC can help to determine the UHI phenomenon and its urban ecological degradations in the study area.

5 Conclusions

In this study, geospatial analyses have been carried out to examine the relationship between UHI and LUCC in Osmaniye city. The analyses were based on the interpretation of the remote sensing images and data, by which the LUCC impacts on land surface temperature increase were estimated. In order to select proper satellite images, the most uniform atmosphere condition was used based on the local level. Some limitations with these satellite images were that choosing satellite images with appropriate conditions of topography and green spaces can be the strain for the study area. The period of satellite data used during the analysis was also limited since this is the first study in Osmaniye city examining the impacts of LUCC on UHI dissemination, and may enlighten future researches focusing on environmental monitoring and assessment of the study area.

Land surface temperature is mainly impacted by external factors such as heat originating human activity, surface area of the landscape, and LUCC. For the present study, UHI is substantially influenced by increased urbanized areas and vegetative degradation such as the decrease in forest cover in city layout. The temperature patterns derived from UHI phenomenon can significantly help arrange local plans to determine which area requires the increase in vegetative cover for the study area. The findings of this study have also revealed additional scientific technique for city planners to identify and locate total built-up areas which lead to the increase in land surface temperature in Osmaniye city.

Furthermore, the difference between land surface temperature in 2000 and 2018 can be impacted by many factors, including season of satellite data acquisition, topography of the landscape, and methods used for classifying land-use categories of the Osmaniye city. Another important factor is the impacts of impervious surface cover density around the urban–rural gradient on land surface temperature which could not be examined for the present study due to insufficient data. Therefore, these categories need to be addressed for future studies along with the analyses and comparison of outcomes across different study areas. It is suggested that policymakers and urban planners should pay attention to alleviate the UHI effects by clustering vegetative cover and equally dispersing total built-up structures so that urban areas can be healthier and more sustainable in the future.

Acknowledgements The author wishes to thank Dr. Filiz Güneysu Atasoy for compiling the data and anonymous reviewers for their constructive comments.

References

- Agbor, C. F., & Makinde, E. O. (2018). Land surface temperature mapping using geoinformation techniques. *Geoinformatics FCE CTU*, 17(1), 17.
- Atasoy, M. (2018). Monitoring the urban green spaces and landscape fragmentation using remote sensing: A case study in Osmaniye, Turkey. *Environmental Monitoring and Assessment*, 190(12), 713.
- Atasoy, M., Anderson, C. J., & Atasoy, F. G. (2018). Evaluating the distribution of invasive woody vegetation around riparian corridors in relation to land use. *Urban Ecosystems*, 21(3), 459–466.
- Bilgili, B. C., Şahin, Ş., Yılmaz, O., Gürbüz, F., & Arıcı, Y. K. (2013). Temperature distribution and the cooling effects on three urban parks in Ankara, Turkey. *International Journal of Global Warming*, 5(3), 296. <https://doi.org/10.1504/ijgw.2013.055364>.
- Bokaie, M., Zarkesh, M. K., Arasteh, P. D., & Hosseini, A. (2016). Assessment of Urban Heat Island based on the relationship between land surface temperature and land use/land cover in Tehran. *Sustainable Cities and Society*, 23, 94–104. <https://doi.org/10.1016/j.scs.2016.03.009>.
- Büyükkbeşe, T., & Aslan, H. (2019). Psikolojik sermaye ve duygusal emeğin örgütsel bağlılık üzerindeki etkisi. *İşletme Araştırmaları Dergisi*, 11(2), 949–963.
- Chander, G., Markham, B. L., & Helder, D. L. (2009). Summary of current radiometric calibration coefficients for Landsat MSS, TM, ETM+, and EO-1 ALIsensors. *Remote Sensing of Environment*, 113(5), 893–903.
- Chen, Y., Wang, J., & Li, X. (2002). A study on urban thermal field in summer based on satellite remote sensing. *Remote Sensing for Land and Resources*, 4, 55–59.
- Chen, X., Zhao, H., Li, P., & Yin, Z. (2006). Remote sensing image-based analysis of the relationship between urban heat island and land use/cover changes. *Remote Sensing of Environment*, 104(2), 133–146. <https://doi.org/10.1016/j.rse.2005.11.016>.
- Chun, B., & Guldmann, J. (2014). Spatial statistical analysis and simulation of the urban heat island in high-density central cities. *Landscape and Urban Planning*, 125, 76–88. <https://doi.org/10.1016/j.landurbplan.2014.01.016>.
- Congalton, R. G. (1991). A review of assessing the accuracy of classifications of remotely sensed data. *Remote Sensing of Environment*, 37(1), 35–46.
- Deosthali, V. (2000). Impact of rapid urban growth on heat and moisture islands in Pune City, India. *Atmospheric Environment*, 34, 2745–2754.
- Dwivedi, A., & Mohan, B. (2018). Impact of green roof on micro climate to reduce Urban Heat Island. *Remote Sensing Applications: Society and Environment*, 10, 56–69. <https://doi.org/10.1016/j.rsase.2018.01.003>.
- El-Hattab, M., Amany, S. M., & Lamia, G. E. (2017). Monitoring and assessment of urban heat islands over the Southern region of Cairo Governorate, Egypt. *The Egyptian Journal of Remote Sensing and Space Science*. <https://doi.org/10.1016/j.ejrs.2017.08.008>.
- Estoque, R. C., & Murayama, Y. (2015). Classification and change detection of built-up lands from Landsat-7 ETM+ and Landsat-8 OLI/TIRS imageries: A comparative assessment of various spectral indices. *Ecological Indicators*, 56, 205–217. <https://doi.org/10.1016/j.ecolind.2015.03.037>.

- Estoque, R. C., Murayama, Y., & Myint, S. W. (2017). Effects of landscape composition and pattern on land surface temperature: An urban heat island study in the megacities of Southeast Asia. *Science of the Total Environment*, 577, 349–359. <https://doi.org/10.1016/j.scitotenv.2016.10.195>.
- Feizizadeh, B., Blaschke, T., Nazmfar, H., Akbari, E., & Kohbanani, H. R. (2013). Monitoring land surface temperature relationship to land use/land cover from satellite imagery in Maraqeh County, Iran. *Journal of Environmental Planning and Management*, 56(9), 1290–1315.
- Fu, P., & Weng, Q. (2017). Responses of urban heat island in Atlanta to different land-use scenarios. *Theoretical and Applied Climatology*, 133(1–2), 123–135. <https://doi.org/10.1007/s00704-017-2160-3>.
- Fung, T., & Siu, W. (2000). Environmental quality and its changes, an analysis using NDVI. *International Journal of Remote Sensing*, 21(5), 1011–1024.
- Güngör, S., & Polat, A. T. (2017). The evaluation of the urban parks in Konya province in terms of quality, sufficiency, maintenance, and growth rate. *Environmental Monitoring and Assessment*, 189(4), 172.
- Hosseini, A., Pourahmad, A., & Pajoohan, M. (2015). Assessment of institutions in sustainable urban-management effects on sustainable development of Tehran: Learning from a developing country. *Journal of Urban Planning and Development*, 142(2), 05015009.
- Howard, L. (1833). Climate of London deduced from meteorological observation. *Harvey and Darton*, 1(3), 1–24.
- Kilinc, G., & Gulseroy, N. Z. (2011). Evaluation of the potential for districts/counties to become provinces with respect to the level of urbanization in Turkey. *European Planning Studies*, 19(8), 1557–1580.
- Laosuwan, T., & Sangpradit, S. (2012). Urban heat island monitoring and analysis by using integration of satellite data and knowledge based method. *International Journal of Development and Sustainability*, 1(2), 99–110.
- Li, J., Song, C., Cao, L., Zhu, F., Meng, X., & Wu, J. (2011). Impacts of landscape structure on surface urban heat islands: A case study of Shanghai, China. *Remote Sensing of Environment*, 115(12), 3249–3263. <https://doi.org/10.1016/j.rse.2011.07.008>.
- Li, H., Zhou, Y., Li, X., Meng, L., Wang, X., Wu, S., et al. (2018). A new method to quantify surface urban heat island intensity. *Science of the Total Environment*, 624, 262–272. <https://doi.org/10.1016/j.scitotenv.2017.11.360>.
- Lobo, A., Legendre, P., Rebollar, J. L. G., Carreras, J., & Ninot, J. M. (2004). Land cover classification at a regional scale in Iberia: Separability in a multi-temporal and multi-spectral data set of satellite images. *International Journal of Remote Sensing*, 25(1), 205–213.
- Mirzaei, P. A. (2015). Recent challenges in modelling of urban heat island. *Sustainable Cities and Society*, 19, 200–206.
- Nastran, M., Kobal, M., & Eler, K. (2018). Urban heat islands in relation to green land use in European cities. *Urban Forestry & Urban Greening*. <https://doi.org/10.1016/j.ufug.2018.01.008>.
- Osmaniye Municipality. (2018). *The municipality of Osmaniye City*. Retrieved July 31, 2018 from <http://osmaniye-bld.gov.tr/>
- Soysal, A., Özçalıcı, M., & Güneysu, F. (2010). The contribution of undergraduate students to region economics: A research on undergraduate students. In *1st International Border Trade Congress* (Vol. 1(1)). Retrieved January 15, 2019 from http://iibf.kilis.edu.tr/bordertrade/files/Kongre_kitapcigi.pdf
- Sun, Q., Tan, J., & Xu, Y. (2010). An ERDAS image processing method for retrieving LST and describing urban heat evolution: A case study in the Pearl River Delta Region in South China. *Environmental Earth Sciences*, 59(5), 1047–1055.
- TUIK. (2018). *Turkish Statistical Institute addressed based population registration system*. Retrieved October 15, 2018 from www.tuik.gov.tr/PreIstatistikTablo.do?istab_id=1590.
- Weng, Q., & Lu, D. (2008). A sub-pixel analysis of urbanization effect on land surface temperature and its interplay with impervious surface and vegetation coverage in Indianapolis, United States. *International Journal of Applied Earth Observation and Geoinformation*, 10(1), 68–83.
- Yalcin, G. (2014). Urban activities in the view of the sustainable development. *Procedia Technology*, 12, 566–571.
- Yang, C., He, X., Yan, F., Yu, L., Bu, K., Yang, J., et al. (2017). Mapping the influence of land use/land cover changes on the urban heat island effect—A case study of Changchun. *China Sustainability*, 9(2), 312. <https://doi.org/10.3390/su9020312>.
- Yuan, F., & Bauer, M. E. (2007). Comparison of impervious surface area and normalized difference vegetation index as indicators of surface urban heat island effects in Landsat imagery. *Remote Sensing of Environment*, 106(3), 375–386. <https://doi.org/10.1016/j.rse.2006.09.003>.